

# PD Sliding Mode Controller based Decoupled Aerial Manipulation

Kamel Bouzgou<sup>1,2</sup><sup>a</sup>, Laredj Benchikh<sup>1</sup><sup>b</sup>, Lydie Nouveliere<sup>1</sup><sup>c</sup>, Yasmina Bestaoui<sup>1</sup><sup>d</sup>  
and Zoubir Ahmed-Foith<sup>2</sup><sup>e</sup>

<sup>1</sup>IBISC, Univ. Evry, Université Paris-Saclay, 91025, Evry, France

<sup>2</sup>LEPESA Laboratory, Faculty of Electrical Engineering, Department of Electronics, USTO-MB, 31000 Oran, Algeria

**Keywords:** Aerial Manipulation, Decoupled Dynamic System, SMC, Sliding Mode Control, PD-SMC.

**Abstract:** This paper presents the design of 3-Dof multi-link robot arm that is mounted on the multirotor. To be considered the dynamic characteristics of the manipulation platform, the decoupled dynamic models of the system are derived. The main advantage of the first joint is introduced for more robustness and stability during hovering. The PID controller will be implemented for position and attitude of multirotor control, whereas, a sliding mode controller will be designed for a manipulator robot, which is then compared with the sliding surface that has been integrated with the proportional-derivative (PD) controller. The performance of the proposed technique is demonstrated through a simulation using Simulink and Matlab environment.

## 1 INTRODUCTION

Unmanned aerial manipulators (UAMs) are used for mobile manipulations thanks to their mobility which enables a simple hovering to aggressive manoeuvres. It has emerged a need for the interaction of that UAVs with the environment that is not easily accessible by humans, for this aim, the researchers have used this structure for transporting, manipulation and grasping tasks. Moreover, the control of these aerial manipulator is a very challenging problem, considering that such system is under-actuation and the coupled dynamics between the two different platforms, and the contact with the environment during manipulation. Several survey papers deal with projects that the multi-link robotic arm attached to the UAV for manipulation tasks are used, the dynamic formalism and control technique developed. Authors in (Bouzgou et al., 2019a) have classified aerial manipulator systems based on aerial vehicles and the attached arm kind. For the simple grasping task, a magnet attached to the UAV is presented in (Escareno et al., 2014). A single Dof to push an object in the desired direction, in (Srikanth et al., 2011; Yeol et al., 2017) is designed

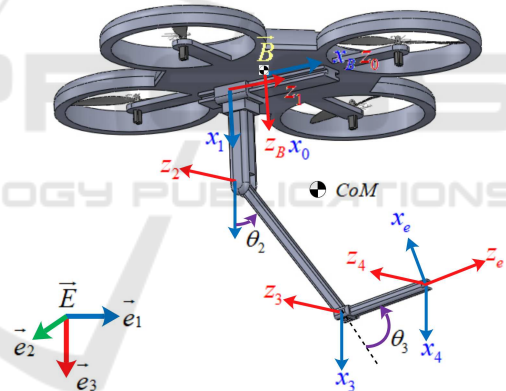





Figure 1: The structure of Q-PRR with principal frames.


as a non-prehensile manipulation and tentacle system.


The most structure of aerial manipulator arm is when a 2-Dof robot arm is mounted (Aydemir et al., 2015; Kim et al., 2013), that number of dof can help users to avoid a singularity region in the manipulator arm workspace. A 3-Dof manipulator arm as revolute joints is used in (Mello et al., 2015), when 4-Dof multi-link manipulator arm is presented in (Jimenez-Cano et al., 2017) as a serial robot placed at the upper part of the UAV for bridge inspection. In (Koncak et al., 2013) authors are used a 5-Dof manipulator robot for environment interaction. An industrial manipulator as a redundant robot arm with  $n > 6$  is used in (Huber et al., 2013) aerial manipulation with a 7-Dof based on a main-tail-rotor helicopter, in (Danko

<sup>a</sup> <https://orcid.org/0000-0003-2374-2149>

<sup>b</sup> <https://orcid.org/0000-0002-4617-399X>

<sup>c</sup> <https://orcid.org/0000-0003-0027-7192>

<sup>d</sup> <https://orcid.org/0000-0001-7716-5952>

<sup>e</sup> <https://orcid.org/0000-0003-3121-9964>

and Oh, 2014) the Hyper-redundant manipulator is presented as 9-Dof for a wide reachable workspace. A delta structure fixed on side of UAV was introduced in (Fumagalli et al., 2014), when a parallel robot is used in (Cho and Shim, 2017; Danko et al., 2015). For an object interaction and manipulation applying forces and torques, a dual 4-dof arm mounted on UAV is presented in (Korpela et al., 2013).

Researchers in (Ruggiero et al., 2015), have developed a structure with a moving battery of the UAV in one direction in order to hold the Multirotor CoG as close as possible to the vertical axis, The drawback of such structure is that battery movement is bounded when the end-effector tried to reach the desired position and battery position cannot always ensure the alignment of CoM of UAV and robot arm. A new aerial manipulator with a 3-Dof is developed in this paper (Bouzgou et al., 2019b), the alignment of CoG of whole system can be ensured with a simple movement of a prismatic joint along x-axis Figure 1. wide workspace with this design and offering large possible configurations of the robot arm for a desired position and attitude without losing the optimum location of the Q-PRR CoG (Bouzgou and Ahmed-Foithi, 2015).

An adaptive sliding controller based on a traditional Lagrange modeling method was proposed (Kim et al., 2013), An augmented adaptive sliding controller based on a closed-chain robot dynamics was presented for cooperative transportation of multiple (Lee et al., 2015) online estimation of objects based on an augmented adaptive sliding controller was proposed.

## 2 MODELING

The configuration of the proposed aerial manipulator consists of two parts, the multi-rotor with the number of rotors that  $n_r = 4$  that can be called with the letter "Q" for Quadrotor more details see (Bouzgou et al., 2019a), and the manipulator arm attached to the bottom, whose geometric centers are considered to be in the same  $z$  axis ( $\vec{b}_3$ ) of the mobile frame  $\vec{B}$ . The manipulator consists of three degrees of freedom (3-Dof), Prismatic-Revolute-Revolute joints, called (Q-PRR), the first joint is prismatic and its axis ( $x_1$ ) is parallel to the  $x$ -axis of the multirotor mobile frame  $\vec{B}$ , this joint is considered actuated and it moves along the same axis, and it is bounded on both directions by a value  $r_0$ , the distance between two axes  $x_b$  and  $x_1$  is denoted by ( $d_0$ ), The second and third joints are revolute, their rotation axes ( $z_2$ ) and ( $z_3$ ) are parallel to the ( $y$ ) axis of the  $\vec{B}$  unit, where the manipulator arm movements are considered in the ( $x, z$ )-axis of the  $\vec{B}$

mobile frame. The position of the  $\vec{B}$  fixed frame with respect to the  $\vec{E}$  inertial frame is given by the ( $3 \times 1$ ) vector denoted by  $p_b$ , whereas its orientation denoted by  $R_b$  is represented by the XYZ rotation sequence with the fixed frame axes, and its orientation by the fixed frame axes.

$$R_b = \begin{bmatrix} c_\theta c_\psi & s_\phi s_\theta c_\psi - c_\phi s_\psi & c_\phi s_\theta c_\psi + s_\phi s_\psi \\ c_\theta s_\psi & s_\phi s_\theta s_\psi + c_\phi c_\psi & c_\phi s_\theta s_\psi - s_\phi c_\psi \\ -s_\theta & s_\phi c_\theta & c_\phi c_\theta \end{bmatrix} \quad (1)$$

where  $s_* = \sin(*)$ ,  $c_* = \cos(*)$ , Let  $R_e^b$  be the orientation matrix of the end-effector attached frame, and  $p_e^b = [x_{eb} \ y_{eb} \ z_{eb}]^T$  the position vector of the origin with respect to  $\vec{B}$  fixed frame, and the absolute position vector and orientation matrix of the end-effector with respect to  $\vec{E}$ , is given by the  $p_e = [x_e \ y_e \ z_e]^T$  and  $R_e$ , respectively, where the pair  $(p_b, R_b) \in SE(3)$  denotes the vector position given by  $p_b = [x_b \ y_b \ z_b]^T$ , and the orientation matrix of the multirotor with respect to the inertial frame  $\vec{E}$ .

The position and orientation equations of end-effector expressed in  $\vec{E}$  are written as follows:

$$p_e = p_b + R_b p_e^b \quad (2)$$

$$R_e = R_b R_e^b \quad (3)$$

By denoting with  $\dot{\phi}_b$  the time derivative of  $\phi_b$ .

$$\omega_b = T(\phi_b) \dot{\phi}_b \quad (4)$$

Where  $T(\phi_b)$  is the transformation matrix between the time derivative of the Euler angles  $\phi_b$  and the angular velocity of the multirotor  $\omega_b$ .

$$T(\phi_b) = \begin{bmatrix} 1 & 0 & -s_\theta \\ 0 & c_\phi & s_\phi c_\theta \\ 0 & -s_\phi & c_\phi c_\theta \end{bmatrix} \quad (5)$$

By differentiating (2), (3) and with taking into account (4), the translational and angular velocities of the end-effector with respect to  $\vec{E}$  can be written as follows:

$$\dot{p}_e = \dot{p}_b - R_b \dot{p}_{eb}^b T(\phi_b) \dot{\phi}_b + R_b \dot{p}_{eb}^b \quad (6)$$

$$\omega_e = T(\phi_b) \dot{\phi}_b + R_b \omega_{eb}^b \quad (7)$$

Where  $\dot{p}_b, \omega_b$  are the linear and angular velocities of the mobile frame  $\vec{B}$  with respect to the  $\vec{E}$  frame, respectively, and  $\dot{p}_{eb}^b, \omega_{eb}^b$  are the translational and angular velocities of the end-effector with respect to the mobile frame  $\vec{B}$ . ( $\hat{\cdot}$ ), the hat map that transforms a vector in  $\mathbb{R}^3$  to  $(3 \times 3)$  Skew-symmetric matrix such that  $\hat{x}y = x \times y, \forall x, y \in \mathbb{R}^3$  (Kamel et al., 2017).

The dynamic model of Q-PRR can be derived by considering the Lagrange formulation in details in (Lippiello and Ruggiero, 2012). The function of Lagrangian is then expressed by  $\mathcal{L} = \mathcal{E} - \mathcal{U}$  where  $\mathcal{E}$ ,

$\mathcal{U}$  denote the kinematics and potential energy of the whole system, respectively. The Lagrange equations are given by

$$\frac{d}{dt} \frac{\delta \mathcal{L}}{\delta \dot{\xi}_i} - \frac{\delta \mathcal{L}}{\delta \xi_i} = u + u_{ext} \quad (8)$$

Where  $i = 1, \dots, 6 + n$  is the  $i$ -th coordinate of  $\xi$ , and  $u_i$  is the  $((6 + n) \times 1)$  vector of generalized forces and torques, and  $u_{ext}$  denotes the vector of external disturbance forces and torques. the dynamic model of the global system can be written as

$$B(\xi)\ddot{\xi} + C(\xi, \dot{\xi})\dot{\xi} + G(\xi) = u + u_{ext} \quad (9)$$

Where  $G$  is a  $((6 + n) \times 1)$  vector of gravitational terms given by deriving the potential energy as  $G(\xi) = \frac{\delta p}{\delta \xi}$ . And  $C$  is the matrix of Coriolis and centrifugal terms. more details see (Bouzgou et al., 2019b).

$u_i$  is the vector of generalized forces at the  $i$ -th joint level.  $\tau_b$  is the vector of torques composed with  $\tau_\phi$ ,  $\tau_\theta$  and  $\tau_\psi$  generated by the system computed around  $x, y$  and  $z$  axes respectively. Let  $\mu$  be the vector of the force  $f_{r_0}$  applied to the prismatic joint and  $\tau_{\theta_2}$ ,  $\tau_{\theta_3}$  torques applied by the revolute joint of the robot arm.

$$u = \begin{bmatrix} u_{f_b} \\ u_{\tau_b} \\ u_\mu \end{bmatrix} = \begin{bmatrix} R_b f_b \\ R_b^T T_b \tau_b \\ \mu \end{bmatrix} = \text{diag}(R_b, Q, I_n)$$

$$f_b = \begin{bmatrix} 0 \\ 0 \\ f_{bz} \end{bmatrix}, \quad \tau_b = \begin{bmatrix} \tau_\phi \\ \tau_\theta \\ \tau_\psi \end{bmatrix}, \quad \mu = \begin{bmatrix} f_{r_0} \\ \tau_{\theta_2} \\ \tau_{\theta_3} \end{bmatrix}$$

$$\begin{bmatrix} f_{bz} \\ \tau_b \end{bmatrix} = \begin{bmatrix} 1 & 1 & 1 & 1 \\ 0 & l & 0 & -l \\ -l & 0 & l & 0 \\ c & -c & c & -c \end{bmatrix} \begin{bmatrix} f_1 \\ f_2 \\ f_3 \\ f_4 \end{bmatrix} \quad (10)$$

Where  $l$  is the distance from each motor to the multirotor centre of mass. When  $c$  is the drag factor. Since  $B(\xi_i)$  is symmetric  $B_{ij} = B_{ji}^T$ , and Let the matrices  $M_{pp}$ ,  $M_{p\phi}$ ,  $M_{pq}$ ,  $M_{\phi\phi}$ ,  $M_{\phi q}$ ,  $M_{qq}$  be defined by partitioning the mass matrix and by according to the equation defined in Equation 9 the decoupled dynamic model for the overall system is presented and a sub-matrices are given from that equation and can be rewrite as follows

$$B(\xi_i) = \begin{bmatrix} B_{pp} & B_{p\phi} & B_{pq} \\ B_{p\phi}^T & B_{\phi\phi} & B_{\phi q} \\ B_{pq}^T & B_{\phi q}^T & B_{qq} \end{bmatrix} \quad (11)$$

$$C(\xi, \dot{\xi}) = \begin{bmatrix} C_p \\ C_\phi \\ C_q \end{bmatrix}, \quad G(\xi_i) = \begin{bmatrix} G_p \\ G_\phi \\ G_q \end{bmatrix}$$

The dynamic modeling of the decoupled system is presented as follows For the multirotor, a new coordinate joint can be defined as a part of the generalized coordinates  $x_i$  such that  $q_m = [p_b \ \phi_b]^T$ . Multirotor motion equations Equations to respect the Lagrange formalism in Equation 9 and the decomposition of the  $B, C$  and  $G$  matrices can be defined as follows

$$B_{pp}\ddot{p}_b + B_{p\phi}\ddot{\phi}_b + C_p\dot{p}_b + G_p + B_{pq}\ddot{q}_{eb} = u_{f_b} \quad (12)$$

$$B_{p\phi}^T\ddot{p}_b + B_{\phi\phi}\ddot{\phi}_b + C_\phi\dot{\phi}_b + G_\phi + B_{\phi q}\ddot{q}_{eb} = u_{\tau_b} \quad (13)$$

$$B_{pq}^T\ddot{p}_b + B_{\phi q}^T\ddot{\phi}_b + C_q\dot{q}_{eb} + G_q + B_{qq}\ddot{q}_{eb} = u_\mu \quad (14)$$

From the equation 12 and 13, the dynamic model can be simplified with taking into account the decoupled terms. Rewrite that with the model defined in (Kamel et al., 2017), where  $M_p = B_{pq}\ddot{q}_{eb}$ ,  $M_\phi = B_{\phi q}\ddot{q}_{eb}$  and  $M_q = B_{pq}^T\ddot{p}_b + B_{\phi q}^T\ddot{\phi}_b \in \mathbb{R}^{3 \times 1}$ , such as  $M_p = [M_x \ M_y \ M_z]$  and  $M_{\phi_b} = [M_\phi \ M_\theta \ M_\psi]$ . Equations becomes as

$$m\ddot{x} = (c_\phi s_\theta c_\psi + s_\phi s_\psi)u_1 - M_x \quad (15)$$

$$m\ddot{y} = (c_\phi s_\theta s_\psi - s_\phi c_\psi)u_1 - M_y \quad (16)$$

$$m\ddot{z} = (c_\phi c_\theta)u_1 - mg - M_z \quad (17)$$

$$I_x\ddot{\phi} = \dot{\theta}\psi(I_y - I_z) - J_r\dot{\theta}\Omega_r + lu_2 - M_\phi \quad (18)$$

$$I_y\ddot{\theta} = \dot{\phi}\psi(I_z - I_x) - J_r\dot{\psi}\Omega_r + lu_3 - M_\theta \quad (19)$$

$$I_z\ddot{\psi} = \dot{\phi}\dot{\theta}(I_x - I_y) + u_4 - M_\psi \quad (20)$$

where,  $\Omega_r = (\omega_2 + \omega_4 - \omega_1 - \omega_3)$ ,  $I_x$ ,  $I_y$ ,  $I_z$  are the inertia matrix terms and  $m$  the multirotor mass. The dynamic modeling of the robot arm is defined using a Lagrange Formalism depicted in Equation 9, where the jacobians matrix are defined by using a Denavit-Hartenberg method depicted in (Bouzgou and Ahmed-Foitih, 2014) and its equation of movement can be presented as follow

$$f_{r_0} = (m_1 + m_2 + m_3)\ddot{r}_0$$

$$+ \frac{1}{2} \left( m_3 \left( \frac{1}{2} d_3 c_{\theta_2 + \theta_3} + d_2 c_{\theta_2} \right) + d_2 m_2 c_{\theta_2} \right) \ddot{\theta}_2$$

$$+ \frac{1}{2} (d_3 m_3 c_{\theta_2 + \theta_3}) \ddot{\theta}_3$$

$$- \frac{1}{2} \left( 2m_3 \left( \frac{1}{2} d_3 s_{\theta_2 + \theta_3} + d_2 s_{\theta_2} \right) + d_2 m_2 s_{\theta_2} \right) \dot{\theta}_2^2$$

$$- \frac{1}{2} d_3 m_3 s_{\theta_2 + \theta_3} \dot{\theta}_3^2$$

$$- d_3 m_3 s_{\theta_2 + \theta_3} \dot{\theta}_2 \dot{\theta}_3$$

$$- g(m_1 + m_2 + m_3) \quad (21)$$

$$\begin{aligned}
 \tau_{\theta_2} = & \left( m_3 \left( \frac{1}{2} d_3 c_{\theta_2 + \theta_3} + d_2 c_{\theta_2} \right) + \frac{1}{2} d_2 m_2 c_{\theta_2} \right) \ddot{r}_0 \\
 & + \left( I_{y3} + I_{z2} + \frac{1}{2} m_2 d_2^2 + d_2^2 m_3 + \frac{1}{4} m_3 d_3^2 + d_2 d_3 m_3 c_{\theta_3} \right) \ddot{\theta}_2 \\
 & + \left( \frac{1}{4} m_3 d_3^2 + \frac{1}{2} d_2 d_3 m_3 c_{(\theta_3)} + I_{y3} \right) \ddot{\theta}_3 \\
 & - \frac{1}{2} \left( I_{x3} s_{2\theta_2 + 2\theta_3} - I_{z3} s_{2\theta_2 + 2\theta_3} + d_2 d_3 m_3 s_{\theta_3} \right) \dot{\theta}_3^2 \\
 & \quad - d_2 d_3 m_3 s_{\theta_3} \dot{\theta}_2 \dot{\theta}_3 \\
 & - g \left( m_3 \left( \frac{1}{2} d_3 c_{\theta_2 + \theta_3} + d_2 c_{\theta_2} \right) + \frac{1}{2} d_2 m_2 c_{\theta_2} \right) \quad (22)
 \end{aligned}$$

$$\begin{aligned}
 \tau_{\theta_3} = & \frac{1}{2} d_3 m_3 c_{\theta_2 + \theta_3} \ddot{r}_0 \\
 & + \left( I_{y3} + \frac{1}{4} m_3 d_3^2 + \frac{1}{2} d_2 d_3 m_3 c_{\theta_3} \right) \ddot{\theta}_2 \\
 & + \left( I_{y3} + I_{z3} + \frac{1}{4} m_3 d_3^2 + I_{x3} s_{\theta_2 + \theta_3}^2 - I_{z3} s_{\theta_2 + \theta_3}^2 \right) \ddot{\theta}_3 \\
 & \quad + \frac{1}{2} d_2 d_3 m_3 s_{(\theta_3)} \dot{\theta}_2^2 \\
 & + \frac{1}{2} \left( 2I_{x3} c_{\theta_2 + \theta_3} s_{\theta_2 + \theta_3} - 2I_{z3} c_{\theta_2 + \theta_3} s_{\theta_2 + \theta_3} \right) \dot{\theta}_3^2 \\
 & \quad + s_{2\theta_2 + 2\theta_3} (I_{x3} - I_{z3}) \dot{\theta}_2 \dot{\theta}_3 \\
 & \quad - \frac{1}{2} d_3 g m_3 c_{\theta_2 + \theta_3} \quad (23)
 \end{aligned}$$

Where,  $c_* = \cos(*)$ ,  $s_* = \sin(*)$ . These equations can be rewritten as a matrix forms regarding to the Equation 14.

### 3 CONTROL DESIGN

This section describes the design of the controller for the decoupled system, it is composed into three parts, attitude control of the multirotor as a function of the position of the desired center of gravity; and control of the manipulator arm when the system reaches the target position point, the PID proportional integral derivative controller is used for the multirotor and the sliding mode technique for the manipulator arm and then it will be improve when the PID will be added in parallel. Figure 2 shows the diagram of the control strategy.

From the dynamic equations , we have a decoupled system where the translational accelerations don't depend on angular acceleration, from the first three equations we can extract the pitch and roll angles when we introduce the desired position and attitude. From equations 15, 16, 17,  $\theta$  and  $\phi$  can be computed and its depended on multirotor position vector

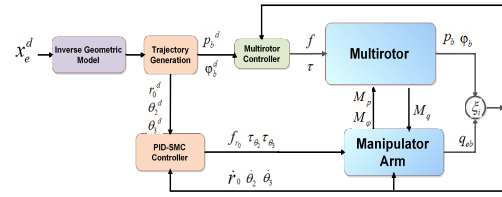


Figure 2: Diagram of the control strategy.

and altitude  $[x \ y \ z \ \psi]$ , therefore, it can be writing as follows

$$\tan(\theta) = \frac{\left( \ddot{x} + \frac{M_x}{m} \right) c_\psi + \left( \ddot{y} + \frac{M_y}{m} \right) s_\psi}{\ddot{z} + g + \frac{M_z}{m}} \quad (24)$$

$$\sin(\phi) = \frac{\left( \ddot{x} + \frac{M_x}{m} \right) s_\psi + \left( \ddot{y} + \frac{M_y}{m} \right) c_\psi}{\sqrt{\left( \ddot{x} + \frac{M_x}{m} \right)^2 + \left( \ddot{y} + \frac{M_y}{m} \right)^2 + \left( \ddot{z} + g + \frac{M_z}{m} \right)^2}} \quad (25)$$

When the reference value for the roll and pitch angles has been calculated, the control inputs of those angles can be determined, and the feedback of the speed time derivative will be required to determine the input vector, in the continuous time, the parallel PID controller is defined, it have a following form

$$u(t) = K_{p\zeta} e(t) + K_{i\zeta} \int_0^t e(\tau) d\tau + K_{d\zeta} \frac{de(t)}{dt} \quad (26)$$

$\zeta$  is the variable to be controlled.  $\zeta \in \{x, y, z, \phi, \theta, \psi\}$  Where,  $e(t) = \zeta_d - \zeta$ , is the error between the desired and measured value of  $\zeta$  and  $K_{p\zeta}$ ,  $K_{i\zeta}$  are Proportional and Integral gain, respectively.

#### 3.1 Manipulator Arm Controller

For the manipulator arm, sliding mode control strategy will be presented, the main idea of this approach can be presented as follows.

Considering the non-linear n-order object defined as

$$x^{(n)}(t) = f(x, t) + u(t) \quad (27)$$

where  $x$  is the state variable,  $u$  is the control law. Let be  $e$  is the error between desired and measured value of  $x$ , such as  $e = x_{des} - x$ , let be  $s = 0$  as a sliding surface defined by

$$s = e^{(n-1)} + \lambda_1 e^{(n-2)} + \dots + \lambda_{n-2} \dot{e} + \lambda_{n-1} e \quad (28)$$

Where  $\lambda$  is the coefficient of the sliding surface. Derivative the equation 28, it can write

$$\dot{s} = e^n + \lambda_1 e^{(n-1)} + \dots + \lambda_{n-2} e^2 + \lambda_{n-1} \dot{e} \quad (29)$$

Using Equation 27 and with choosing the input control vector  $u$  that  $\dot{s} = K \text{sgn}(s)$  with  $K$  is positive defined. Substituting into Equation 29, the following

equation can be rewritten

$$u = -f(x, t) + x_{des}^{(n)} + \lambda_1 e^{(n-1)} + \dots + \lambda_{n-1} \dot{e} + Ksgn(s) \quad (30)$$

$sgn$  is the sign function, applying equation 30 with  $n = 2$  and for three link robot arm  $\ddot{x} = f(x, t) + u(t)$ . The input control law is as follows

$$u(t) = -f(x, t) + q_{des} + \lambda \dot{e} + Ksgn(s) \quad (31)$$

With  $q_{des} = [r_{0,des} \theta_{2,des} \theta_{3,des}]^T$ ,  $\lambda = [\lambda_1 \lambda_2 \lambda_3]^T$  and  $K = [K_1 K_2 K_3]^T$

### 4 SIMULATION AND RESULTS

Simulations were conducted to evaluate the performance of the aerial manipulator in maintaining an end-effector position relative to fixed targets. the desired position of the multirotor is given by  $p_b[m] = [20 \ 30 \ 10]^T$ , and when the roll and pitch angles of the multirotor are considering as zero, the movement of the arm will be started, and the desired trajectory of all joints is given by  $p_{eb} = [0.04 \ 0.6 \ 0.2]^T [m,rad,rad]$  The simulation results are summarized in Figure 3.

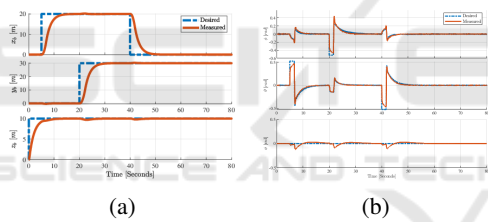


Figure 3: Position of the multirotor centre of gravity in Figure 3a, the orientation of the multirotor fixed frame  $\vec{B}$  to respect to the reference frame  $\vec{E}$  in the Figure 3b.

The position errors of the end-effector can be summarized in the Figure 4.

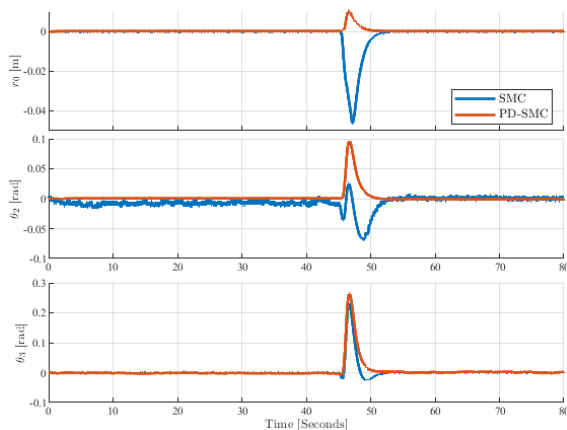


Figure 4: Position Errors of the CoM of Q-PRR.

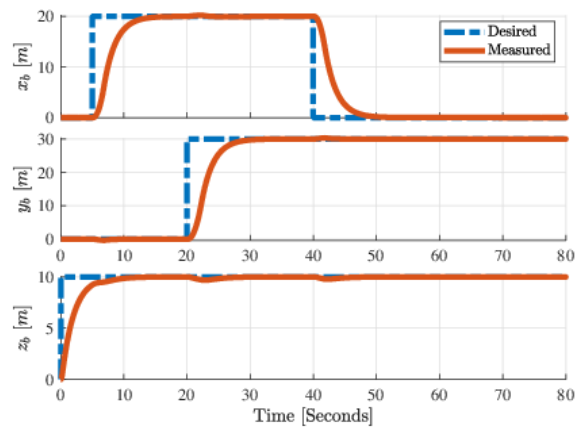


Figure 5: Position of the Center of mass of the Q-PRR.

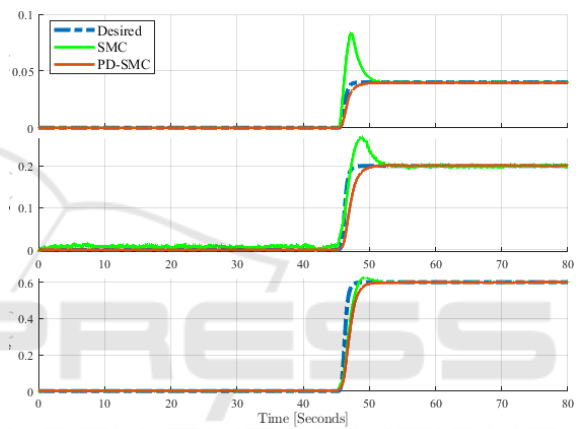


Figure 6: Response of manipulator joints.

### 5 CONCLUSIONS

In this paper, a mathematical model for a decoupled system (multirotor and robot arm) is presented by using the Denavit-Hartenberg approach for geometric modeling of a manipulator arm, and a Lagrange Formalism for dynamic modeling of both a Multirotor and arm . The system dynamics is decoupled in two separate subsystems, one concerning the position of the center of mass where a PID controller is used to keep a stability of the whole system during hovering, a second subsystem concerning the attitude of the manipulator arm, which the sliding mode controller is used to control each link for a path trajectory between a start point to a desired position of the end-effector. That controller is modified and PD terms are added for the sliding mode blocs in order to improve the output signal and defined good stability of the Q-PRR. Simulation works are presented which validate and show the efficiency of the proposed approach. Future works will present another approach for a dynamic



model by using a SimMechanics and VRML environment (Bouzgou et al., 2014) (Bouzgou et al., 2015).

## REFERENCES

- Aydemir, M., Arıkan, K. B., and İrfanoğlu, B. (2015). Disturbance rejection control of a quadrotor equipped with a 2 dof manipulator. In *Machine Vision and Mechatronics in Practice*, pages 91–103. Springer.
- Bouzgou, K. and Ahmed-Foiti, Z. (2014). Geometric modeling and singularity of 6 dof fanuc 200ic robot. In *Innovative Computing Technology (INTECH), 2014 Fourth International Conference on*, pages 208–214. IEEE.
- Bouzgou, K. and Ahmed-Foiti, Z. (2015). Workspace analysis and geometric modeling of 6 dof fanuc 200ic robot. *Procedia-Social and Behavioral Sciences*, 182:703–709.
- Bouzgou, K., Ahmed-Foiti, Z., and Oran-Algeria, U. M. (2014). Singularity analysis and illustration of inverse kinematic solutions of 6 dof fanuc 200ic robot in virtual environment. *Journal of Intelligent Computing*, 5(3):91–105.
- Bouzgou, K., Amar, R. H. E., and Ahmed-Foiti, Z. (2015). Virtual reality simulation and singularity analysis of 3-rrr translational parallel robot. In *Innovative Computing Technology (INTECH), 2015 Fifth International Conference on*, pages 61–66. IEEE.
- Bouzgou, K., Benchikh, L., Nouveliere, L., Bestaoui, Y., and Ahmed-Foiti, Z. (2019a). A new classification and aerial manipulation q-prr design.
- Bouzgou, K., Benchikh, L., Nouveliere, L., Bestaoui, Y., and Ahmed-Foiti, Z. (2019b). A novel aerial manipulation design, modelling and control for geometric com compensation.
- Cho, S. and Shim, D. H. (2017). Development of a vision-enabled aerial manipulator using a parallel robot. *Transaction of the Japan Society for Aeronautical and Space Sciences*, 15(APISAT-2016):a27–a36.
- Danko, T. W., Chaney, K. P., and Oh, P. Y. (2015). A parallel manipulator for mobile manipulating uavs. In *Technologies for Practical Robot Applications (TePRA), 2015 IEEE International Conference on*, pages 1–6. IEEE.
- Danko, T. W. and Oh, P. Y. (2014). Design and control of a hyper-redundant manipulator for mobile manipulating unmanned aerial vehicles. *Journal of Intelligent & Robotic Systems*, 73(1-4):709.
- Escareno, J., Flores, G., Rakotondrabe, M., Romero, H., Lozano, R., and Rubio, E. (2014). Task-based control of a multirotor miniature aerial vehicle having an onboard manipulator. In *Unmanned Aircraft Systems (ICUAS), 2014 International Conference on*, pages 857–863. IEEE.
- Fumagalli, M., Naldi, R., Macchelli, A., Forte, F., Keemink, A. Q., Stramigioli, S., Carloni, R., and Marconi, L. (2014). Developing an aerial manipulator prototype: Physical interaction with the environment. *IEEE robotics & automation magazine*, 21(3):41–50.
- Huber, F., Kondak, K., Krieger, K., Sommer, D., Schwarzbach, M., Laiacker, M., Kosyik, I., Parusel, S., Haddadin, S., and Albu-Schäffer, A. (2013). First analysis and experiments in aerial manipulation using fully actuated redundant robot arm. In *Intelligent Robots and Systems (IROS), 2013 IEEE/RSJ International Conference on*, pages 3452–3457. IEEE.
- Jimenez-Cano, A., Heredia, G., and Ollero, A. (2017). Aerial manipulator with a compliant arm for bridge inspection. In *Unmanned Aircraft Systems (ICUAS), 2017 International Conference on*, pages 1217–1222. IEEE.
- Kamel, B., Yasmina, B., Laredj, B., Benaoumeur, I., and Zoubir, A.-F. (2017). Dynamic modeling, simulation and pid controller of unmanned aerial vehicle uav. In *Innovative Computing Technology (INTECH) Seventh International Conference on*, pages 64–69. IEEE.
- Kim, S., Choi, S., and Kim, H. J. (2013). Aerial manipulation using a quadrotor with a two dof robotic arm. In *Intelligent Robots and Systems (IROS)/RSJ International Conference on*, pages 4990–4995. IEEE.
- Kondak, K., Krieger, K., Albu-Schaeffer, A., Schwarzbach, M., Laiacker, M., Maza, I., Rodriguez-Castano, A., and Ollero, A. (2013). Closed-loop behavior of an autonomous helicopter equipped with a robotic arm for aerial manipulation tasks. *International Journal of Advanced Robotic Systems*, 10(2):145.
- Korpela, C., Orsag, M., Pekala, M., and Oh, P. (2013). Dynamic stability of a mobile manipulating unmanned aerial vehicle. In Germany 2013, I., editor, *Robotics and Automation International Conference on*, pages 4922–4927. IEEE.
- Lee, H., Kim, H., and Kim, H. J. (2015). Path planning and control of multiple aerial manipulators for a cooperative transportation. In *2015 IEEE/RSJ International Conference on Intelligent Robots and Systems (IROS)*, pages 2386–2391. IEEE.
- Lippiello, V. and Ruggiero, F. (2012). Cartesian impedance control of a uav with a robotic arm. *IFAC Proceedings Volumes*, 45(22):704–709.
- Mello, L. S., Aldorno, B., and Raffo, G. V. (2015). Whole-body modeling and control of an unmanned aerial manipulator. In *the XII Brazilian Symposium of Intelligent Automation (XII SBAI). Natal*.
- Ruggiero, F., Trujillo, M. A., and all (2015). A multi-layer control for multirotor uavs equipped with a servo robot arm. In *Robotics and Automation (ICRA), IEEE International Conference on*, pages 4014–4020.
- Srikanth, M. B., Soto, A., Annaswamy, A., Lavretsky, E., and Slotine, J.-J. (2011). Controlled manipulation with multiple quadrotors. In *AIAA Conf. on Guidance, Navigation and Control*.
- Yeol, J. W., Toohey, D., and Hwang, Y.-W. (2017). Design and analysis of a multiple tentacle system for mobile manipulation in micro aerial vehicles. *Procedia Computer Science*, 105:7–13.